PAPER

Rapid multilayer microfabrication for modeling organotropic metastasis in breast cancer

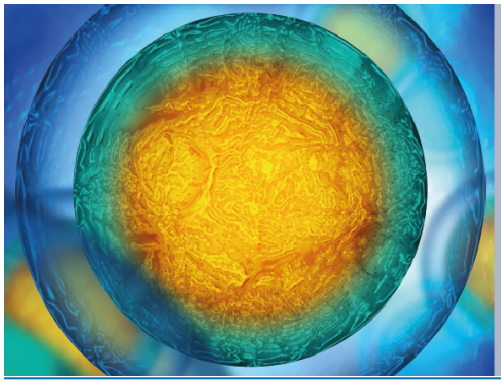

IOP Publishing Biofabrication 13 (2021) 015002 https://doi.org/10.1088/1758-5090/abbd28

Biofabrication

PAPER

Rapid multilayer microfabrication for modeling organotropic metastasis in breast cancer

Tae Joon Kwak and Esak Lee

Nancy E. and Peter C. Meinig School of Biomedical Engineering, Cornell University, Ithaca, NY 14853, United States of America

E-mail: el767@cornell.edu

RECEIVED
8 May 2020

REVISED
29 August 2020

ACCEPTED FOR PUBLICATION
30 September 2020

PUBLISHED
16 October 2020

Keywords: breast cancer, TNBC, tumor-on-a-chip, multilayer, extravasation, engineered vessels, organotropic metastasis

Supplementary material for this article is available online

Abstract

Triple-negative breast cancer (TNBC) is one of the most insidious forms of breast cancer with high rates of metastasis, resulting in major mortalities in breast cancer patients. To better understand and treat TNBC metastasis, investigation of TNBC interactions with blood vasculatures is crucial. Among multiple metastatic processes, a step of TNBC exit from the blood vessels ('extravasation') in the pre-metastatic organs determines the final site of the metastasis. Here, we present a rapid multilayer microfabrication method of transferring a three-dimensional (3D) overhang pattern to a substrate with a sacrificial layer to reconstitute a 3D blood vessel surrounded by the extracellular matrix containing organ-specific parenchymal cells. Bones and lungs are the most common sites of breast cancer metastasis. We modeled organotropic bone and lung metastasis in TNBC by introducing subpopulations of TNBC metastases into a vessel lumen surrounded by osteoblasts, bone marrow derived mesenchymal stem cells, and lung fibroblasts. We found that bone-like microenviroment with osteoblasts and mesenchymal stem cells promoted extravasation of the bone-tropic TNBC cells, whereas the lung-like microenviroment promoted extravasation of the lung-tropic TNBC cells. Given that these organ-specific parenchymal cells do not impact vascular permeability, our results suggest that the parenchymal cells dictate selective extravasation of the bone-tropic or lung-tropic TNBC cells in our system.

1. Introduction

Breast cancer is the most frequently diagnosed cancer in women [1]. Among several breast cancer subtypes, triple-negative breast cancer (TNBC) is the most aggressive form with a high rate of metastasis and a poor prognosis [2]. TNBC does not express three major receptors that are typically expressed in breast cancer: estrogen receptor (*ER*), progesterone receptor (*PR*), and human epidermal growth factor receptor 2 (*HER2*) [2, 3]. The absence of these targetable receptors significantly limits the therapeutic options for treating TNBC [2]. Despite numerous research efforts, TNBC metastasis is still the leading cause of cancer deaths in breast cancer patients.

To better understand and treat TNBC metastasis, we need to look into TNBC interactions with blood vessels. The human blood vasculatures play integral roles in transportation of oxygen and nutrients throughout the body in the normal condition [4]. Breast tumors exploit adjacent blood vessels to maintain their growth by providing oxygen and nutrients to the cancer cells in the tumor mass [5]. To achieve this, breast cancer cells overexpress pro-angiogenic growth factors, such as vascular endothelial growth factor A (VEGF-A) [6] to promote new blood vessel formation in and around the tumor stroma, which is referred to as tumor angiogenesis [7]. However, tumor blood vessels are not only the conduits for blood supply, but also a major route of tumor metastasis to distant organs [8]. In the metastatic process, first, tumor cells must invade local blood vessels and enter the blood circulation ('intravasation'). Next, circulating tumor cells in the blood circulation must survive against harsh conditions like strong shear stress in the blood stream and finally exit from the

blood vessel ('extravasation') and create a new colony ('colonization') in distant sites [9]. Thus, assessing TNBC interactions with blood vasculatures in the tumor and organ microenvironments is fundamental to understand the processes of TNBC metastasis [10].

Physicians have observed the patterns of distant metastasis in breast cancer patients, and discovered that breast cancer highly prefers to certain organs, such as bones, lungs, brains, and livers in the formation of metastases [11, 12]. Among them, the bones and the lungs are the most common organ sites that are metastasized by breast cancer cells [1, 11]. People have studied why certain tumor types prefer to certain organ microenvironments in making new colonies, referring to this phenomenon as organotropic cancer metastasis or organ-specific cancer metastasis [12–15]. To better understand and treat TNBC metastasis, investigating the organ-specific metastasis in the bones and the lungs would be pivotal.

Employing relevant and effective experimental models of TNBC metastasis *in vitro* and *in vivo* would be instrumental to advance our understanding of mechanisms and therapeutic strategies against TNBC. In particular, to understand the organotropism in TNBC metastasis, we need to have models for TNBC extravasation in the pre-metastatic organs. Despite prior uses of animal models in breast cancer research and their contributions to the field [16], it is difficult to predict clinical efficacy and isolate the relative contributions of biological and biophysical factors in these live animal studies, given the genetic discrepancy between different species [17] and inherent complexity of the *in vivo* models [9]. Traditional cell cultures on two-dimensional dishes are highly controllable, but do not recapitulate the three-dimensional (3D) *in vivo* organization [18]. To address this dilemma, microfluidics-based 3D organ-on-a-chip technology employing human cells has been emerging as an alternative *in vitro* platform that better recapitulate behaviors of various tissues and organ functions *in vivo* [19]. In the field of vascular biology, a variety of organ-on-a-chip methods have been developed to mimic human vasculatures and their microenvironments. For instance, needle-based casting method has been used as a conventional tool for fabricating engineered vessels with an ease of obtaining a cylindrical shape in 3D matrices [20–24]. However, there have been technical issues in the method. For example, in order to keep the needle from contacting the bottom surface, a needle buffer layer has to be prepared, and additionally mix of photo resist is required to produce a blocking layer between the needle buffer layer and the needle guide layer [22]. The addition of the photo resist significantly harms the purity of the materials and weakens the bonding strength between the layers, thereby deteriorating the durability of the mold. Alternatively, a needle casting layer and a media reservoir layer were fabricated as separate parts and assembled in the casting process [20, 21]. This method requires an additional PDMS-PDMS bonding process, which is challenging to precisely align the microchannel and the reservoir layer, and often causes defects like fluid leaks between two PDMS layers. The 3D printing method is also widely used to fabricate various, more complex structures [25–29], but the material stacking is difficult to form a clean, smooth cylindrical surface in a high resolution. The flow-induced methods enabled rapid fabrication through a simple structure [30–32], but it is often difficult to predict and achieve precise, reproducible geometries of the vessels because the fabrication largely depends on the viscosity of the materials and variable fluid dynamics. These techniques have demonstrated the potential benefits of micro-sized vascular fabrication and have provided progress in vascular research; however, challenges still remain in the rapid fabrication, easy adaptations, and recapitulation of bona fide human vessels.

Here, we present a rapid multilayer microfabrication method for creating an engineered vasculature in 3D and its crosstalk to TNBC to investigate breast tumor extravasation in distant organs, including bones and lungs, the most common sites of breast cancer metastasis. The method allows the fabrication of a vascular channel with only single casting mold by transferring a 3D overhang pattern made through our novel two-layer SU-8 photolithography process to a substrate with a sacrificial layer. The casting mold with a 3D overhang pattern provides a more reproducible, reliable vascular conduit structure than previous methods described above. We describe the development of the engineered blood vessel on-chip and their applications to understand organotropic metastasis in breast cancer.

2. Materials and methods

2.1. Cell culture

Primary human dermal microvascular blood endothelial cells (BEC, neonatal) were purchased from Lonza. BEC were cultured in EGM-2MV media (Lonza, Switzerland). MDA-MB-231 cells were purchased from ATCC and cultured in DMEM + 10% fetal bovine serum (FBS) + 2 mM L-glutamine + 50 μg ml^{-1} Gentamycin. Metastatic subpopulations of MDA-MB-231, including bone tropic MDA-MB-231 (1833 BoM: we refer to this as 'bone MDA-231') and lung tropic MDA-MB-231 (4175 LM2: we refer to this as 'lung MDA-231') transfected with GFP were donated from Dr Joan Massague at Memorial Sloan Kettering Cancer Center [33, 34]. The bone MDA-231 is a derivative of parental MDA-MB-231 cells that was selected for its ability to metastasize to bone tissues *in vivo* [33]. Briefly, parental MDA-MB-231 cells were inoculated to the heart of mice and metastases to bones

were isolated and enriched. The lung MDA-231 is a derivative of parental MDA-MB-231 cells that was selected for its ability to metastasize to lung tissues *in vivo* [34]. Briefly, parental MDA-MB-231 cells were inoculated orthotopically into mammary fat pads of mice and spontaneous metastases to the lungs were isolated and enriched. The bone and lung MDA-231 were cultured in DMEM + 10% fetal bovine serum (FBS) + 2 mM L-glutamine + 50 μg ml^{-1} Gentamycin. Human osteoblasts were purchased from Lonza and cultured in OGM Osteoblast Growth Media (Lonza). human bone marrow derived mesenchymal stem cells (MSC) and human lung fibroblasts (HLF) were purchased from Lonza and cultured in DMEM + 10% fetal bovine serum (FBS) + 2 mM L-glutamine + 50 μg ml^{-1} Gentamycin. Endothelial cells and all the stromal cells (osteoblasts, MSC, and lung fibroblasts (LF)) were used at passages 3–8, and all the cells were maintained in standard tissue culture incubators at 37 °C, 95% humidity, and 5% CO_2.

2.2. Microfluidic vessel on a chip design

We designed a microfluidic vascular channel device as shown in figure 1(a). The device contains a circular inlet and outlet that can be vice versa for media ports as well as reservoirs. A 20 mm^3 volume extracellular matrix (ECM) hydrogel cavity located in the center of the microfluidic chip device has two ports to access the vessel lumens and serves as a connection area for fluid-handling. Biological network and interaction phenomena between the channel and the ECM can be observed through an optical/fluorescence microscope. The distance between the media ports and the ECM cavity is 4 mm. The design is made using L-edit computer-aided design software (v.15, Tanner EDA by Mentor Graphics Corp., OR, USA), and the ultraviolet (UV) photomasks for three layers are engraved on 5 inch-chromium masks by a laser pattern generator (DWL2000, Heidelberg Instruments, Germany).

2.3. Microfluidic chip device fabrication

The microfabrication photolithography for polydimethylsiloxane (PDMS) mold began with two 100 mm silicon wafer substrates that were previously cleaned with a hot wafer piranha process (HMR900, STEAG HamaTech, Germany) and dehydrated on hot plates for 10 min at 100 °C. One of the wafers was used as a 'pattern wafer' with a sacrificial layer (figures 1(b) and (c)), and another wafer was used as a 'mold wafer' (figure 1(d)). Firstly, approximately 17 nm thick layer of OmniCoat™ was spin-coated on the whole surface of the pattern wafer and then prebaked to reduce the adhesion between the wafer substrate and patterned structures. This layer was used as a sacrificial layer to transfer the SU-8 mold patterns from the pattern wafer to the mold wafer. Next, a 450 μm thick layer of SU-8 2150 (Kayaku advanced materials, MA, USA) for a 100 μm thick gel-top layer and a 350 μm thick needle guide layer was spin-coated and soft-baked. To perform the hundreds of micrometers thick and multi-layered SU-8 structure, extended soft-baking time was processed because the heating decreases the viscosity of the SU-8 by increasing the mobility of the polymer molecules, as well as evaporating contained solvent to hardening of the layer to improve performance of the spin-coating of the next layer [35]. Moreover, considering the low thermal conductivity of the SU-8, slowly ramped (up and down in 2 °C min^{-1}) temperature was proceeded to reduce the internal stress. In addition to the extended soft-baking, it is important to level the wafer in horizontal during the soft-baking process because the gravity participates annihilation of the edge bead. If the wafer is not leveled in horizontal during the soft-baking process, SU-8 flows and causes the thickness variation, resulting in non-uniform contact to the photomask as well as failure in the transferring process because some structures were not entirely in contact during the bonding process. This layer was exposed by two different masks using a UV contact mask aligner (ABM Manual Mask Aligner, ABM-USA Inc. CA, USA) with a 360 nm low-pass filter. For the first UV exposure, the needle guide layer mask was processed with 360 mJ cm^{-2} of exposure which is slightly lower dosages to avoid or minimize cross-linking of the gel-top layer. For the needle guide layer, even if underexposure to this layer occurs, it is rather good to avoid overexposure which creates unnecessary space in the top part of the needle guide layer, since this layer merges with the subsequent needle buffer layer. For the second UV exposure, the gel-top layer mask was processed with 200 mJ cm^{-2} of additional exposure to completely expose the ECM gel casting region, then a post-exposure bake (PEB) was performed. After PEB of the first layer, a 100 μm thick layer of SU-8 100 for the needle buffer layer was spin-coated and soft-baked. The spin-coating of the second layer should be done after the completely cooled-down of the PEB of the first layer because the viscosity of the SU-8 is varying depending on the temperature so that it could cause unwanted thickness difference [36]. The needle buffer layer mask was processed with 450 mJ cm^{-2} of UV exposure. Since the channel structure of this layer is narrower than the channel structure of the previously coated needle guide layer, the needle buffer channel mask was carefully aligned to the center of the needle guide channel structure. This channel merges with the needle guide channel and since the structure of the needle guide channel has a wider structure, proper exposure or slightly overexposure can be performed rather than underexpose to form a complete structure. The needle buffer layer was not performed the PEB for the subsequent transferring (bonding) process.

Simultaneously, a 50 μm thick layer of SU-8 50 (Kayaku advanced materials, MA, USA) for the bonding layer was spin-coated on the mold wafer and

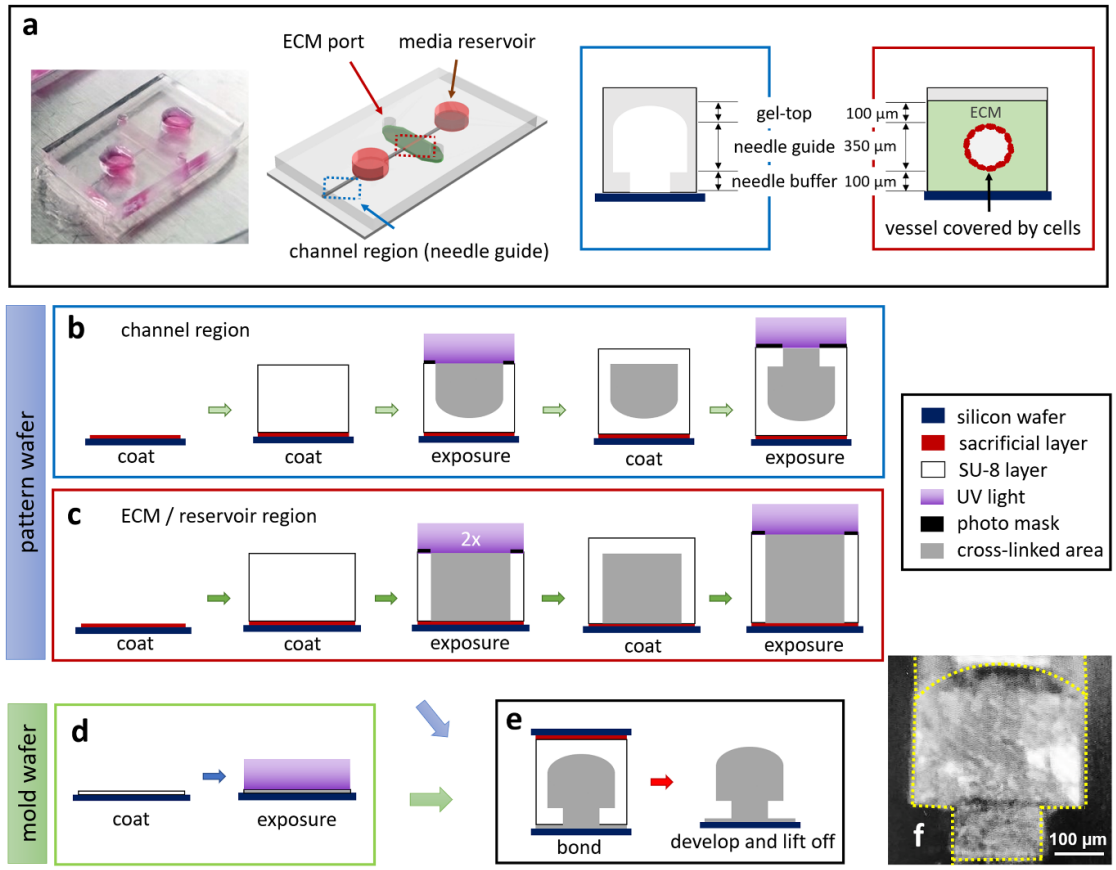

Figure 1. A schematic illustration of the rapid multilayer microfabrication method. (a) A real image of the device and an isometric illustration of the device (left); and in the right, there are cross-section views of the channel region (blue box) and the ECM hydrogel region (red box). (b)-(e) A multi-layer mold fabrication process for the channel region (b) and ECM /reservoir region (c) on the pattern wafer. (d) A flood-exposure is used to form a SU-8 bonding layer on the mold wafer. (e) The two wafers are bonded together by facing during a post-exposure bake (PEB) process and are developed to remove non-crosslinked SU-8 and the sacrificial layer. (f) A cross-section image of a multi-layered overhang structure in the channel region.

soft-baked. The bonding layer was flood-exposed with 450 mJ cm^{-2} of UV exposure without a mask (figure 1(d)). This layer was used as a transparent adhesion layer for the two wafers. Consequently, the two wafers were joint together facing each other, and were performed PEB and developed together (figure 1(e)). After the development, the wafers were washed with IPA to confirm whether additional development is necessary and were developed in an alkaline developer MF319 in order to remove the OmniCoat™ sacrificial layer, completing the transferring process. The surface of the fabricated mold wafer was treated by a monolayer of FOTS ((Tridecafluoro-1,1,2,2-Tetrahydrooctyl)-Trichlorosilane) through the molecular vapor deposition system (MVD 100, Applied MicroStructure Inc. CA, USA) to prevent sticking PDMS to the wafer and SU-8 structures during the PDMS casting process.

The PDMS microfluidic chip was fabricated using a conventional PDMS casting process [37]. A 10:1 ratio of PDMS polymer and cross-linker curing agent (SYLGARD™ 184 Silicone Elastomer Kit, The Dow Chemical Company, MI, USA) were mixed and degassed in a vacuum chamber and were poured to the mold. The mold was left in an oven for more than two hours at 80 °C to harden the PDMS, which is then removed from the mold. Since the overhanging features on the silicon wafer, removing PDMS can crack or damage the SU-8 structure from the mold wafer surface, ethanol was used to swelling the PDMS and lubricate the interface between PDMS and photoresist and assist PDMS removal from the silicon wafer [38]. The removed PDMS microfluidic chip was punched for inlets and outlets of ECM ports and media reservoir region, and bonded to a flat microscope glass slide after a plasma reacted ion etch (RIE) surface treatment (PE-25 Plasma Cleaner, Plasma Etch Inc. NV, USA).

2.4. ECM casting and cell seeding

The microfluidic chip device was plasma treated at 400 W 50 kHz for 5 min with 50 cc min^{-1} of airflow in a vacuum and filled with 0.1% Poly-L-lysine (PLL, #0413, ScienCell Research Laboratories, CA, USA) and was left at least 4 h to coat the surface. Afterward, the microfluidic chip device with the PLL was rinsed with deionized (DI) water three times. Then, 1% glutaraldehyde (G6257, Millipore Sigma,

MO, USA) was added to the ECM port and treated for 15 min. The glutaraldehyde treated microfluidic chip device was rinsed with DI water three times and was soaked overnight in the DI water on an orbital shaker to fully remove any excess glutaraldehyde. A 350 μm diameter of 1% BSA treated casting needles were inserted through the needle guide channel, and collagen I was introduced and polymerized in the center cavity of the device surrounding the casting needle. To polymerize collagen I, 10% of 10x PBS, 2.5% of 1N NaOH, 18.2% of DI water were mixed with 3.57 mg ml^{-1} rat tail collagen I (354 236, Corning, NY, USA) to make the final collagen concentration of 2.5 mg ml^{-1}. Thoroughly mixed the ECM materials were incubated at 37 °C for 1 h and covered with media and incubated overnight. After gelation, needles were removed and human dermal microvascular blood endothelial cells (BEC, Lonza, Switzerland) were seeded in the channel through the media port (reservoir) and allowed to form a monolayer along the wall of the cylindrical channels. The cell-seeded microfluidic chip devices were placed on a platform rocker to generate gravity-driven luminal flow through the channels, providing shear stress at 4–5 dyne cm^{-2}. In order to mimic organ microenvironment, we included 500 000 cells ml^{-1} human osteoblasts, human bone marrow derived mesenchymal stem cells (MSC), and human lung fibroblasts in the ECM when we casted collagen I.

2.5. Immunofluorescence staining and imaging in 3D model

Devices were fixed with 4% paraformaldehyde, permeated and blocked with 3% bovine serum albumin overnight at 4 °C. Primary antibodies detecting VE-cadherin (F11, Santa Cruz Biotechnology, TX, USA, 1:100), CD31 (Agilent Dako, CA, USA, 1:200), GFP (ab6662, Abcam, UK, 1:500) were all incubated in blocking buffer overnight at 4 °C. FITC-conjugated antibody against GFP was used to stain the GFP-expressing breast cancer cells. Primary antibodies were washed overnight using PBS at 4 °C. Secondary antibodies (all from Invitrogen, CA, USA, 1:500), phalloidin (Actin marker, 1:200), and DAPI (Millipore Sigma, MO, USA, 1:500) were subsequently incubated in blocking buffer overnight at 4 °C, and the devices were washed to remove fluorescent background before confocal microscopy. Confocal images were acquired with a Leica SP8 Confocal microscope.

2.6. Statistical analysis

Independent sample populations were compared using unpaired, two-tailed Student's t-test with a normal distribution assumption. $^{*}P < 0.05$ was the threshold for statistical significance. All information regarding the number of experimental repeats and sample sizes were included in figure legends. All data points on the graphs represent average values, and error bars depict SEM.

3. Results and discussion

3.1. Multi-layered microfluidic device mold fabrication

We conducted the multilayer microfabrication method to create a microfluidic organ-on-a-chip engineered tumor-vascular network device. A cross-section view of the channel region of a multilayered device mold is shown in figure 1(f). Unlike the results of traditional top-down straightforward lithography [22], our channel structure, which employs a new method of joining two wafers using a sacrificial layer, clearly shows the overhang boundary of each layer (figure 1(f)). The topside of the microchannel needle guide has an arc shape due to the natural effect of the UV underexposure on the SU-8 (figure 1(f)). To create a more rounded geometry on the wall and top side of the needle guide channel layer for other microfluidic applications, enhanced diffusivity of the UV light, e.g. using a light diffuser, can be applied during the UV mask contact exposure [39, 40].

3.2. Engineered blood vessel formation in the device

We seeded human microvascular BEC in the device to form an engineered blood vessel (figure 2(a)). After seeding the endothelial cells, we introduced fluid shear stress on a rocking platform for 2–3 d, providing them shear stree around at 4–5 dyne cm^{-2}. The device has been fixed and stained with anti-VE-cadherin antibodies to visualize endothelial cell-cell adherens junctions; phalloidin for detecting actins in the cells. We showed appropriate adherens junction formation and stress fiber distribution in the engineered blood vessel (figure 2(b)). Next, we measured the diameter of the 12 individual engineered blood vessels at day 2 to assess reproducibility, and the measured average diameter was 354.93 $\pm$ 4.58 μm. We next tested the diffusive permeability of the engineered blood vessel by introducing FITC-conjugated Dextran (70 kDa, Life Technologies, CA, USA) to the lumen of the engineered blood vessel in living cell condition without fixation, and imaged Dextran diffusion to the matrix in real-time for 4 min. We did not see significant leakage in the timeframe confirming that our BEC channels exhibit a sound barrier function (figure 2(c)). The 4 min diffusion was planned and performed based on our preliminary experiments, showing that 4 min is enough to tell vascular barrier function among different groups of experiments (supplementary figure S1 (available online at https://stacks.iop.org/BF/13/015002/mmedia)). We compared non-cell channels, BEC channels in normal condition, and inflammatory condition (supplementary figure S1). Non-cell channels or BEC channels in the inflammatory condition showed a dramatic burst of dextran diffusion within seconds, compared to the BEC channels in the normal condition (supplementary figure S1).

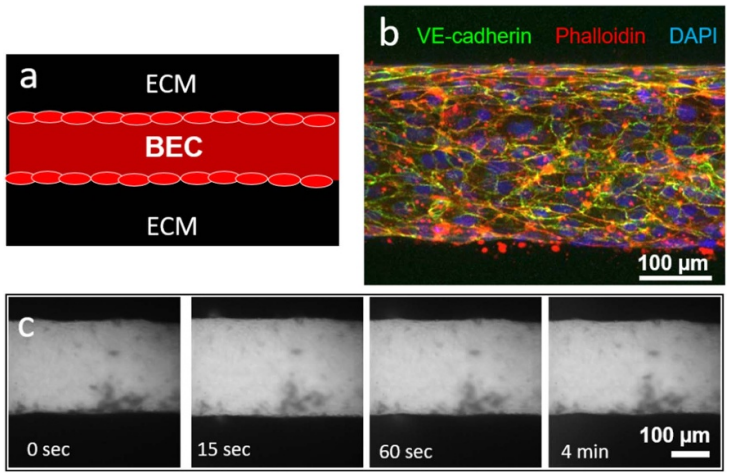

Figure 2. Functionally relevant engineered blood vessels. (a) A schematic of a 3D biomimetic blood vessel surrounded by ECM. (b) Immunostaining of the engineered blood vessels with anti-VE-cadherin antibodies (in green), phalloidin (in red), and DAPI (in blue). (c) The 70 kDa dextran-FITC conjugated was perfused into the engineered vessel lumen and dextran diffusion to the ECM was observed for 4 min to test the barrier function of the engineered blood vessel.

3.3. Breast tumor extravasation in bone microenvironment

Bone is the most common organ in breast cancer metastasis [11]. Upon the results in figure 2, we seeded MDA-MB-231 cells in the channel to show any tumor invasion to the bulk (supplementary figure S2(a)). Based on our initial collagen I (2.5 mg ml^{-1}) condition, we varied the ECM conditions by adding fibronectin (200 μg ml^{-1}) or laminin (200 μg ml^{-1}) to the collagen I. After gelation, needles were removed and MDA-MB-231 breast cancer cells were seeded to form engineered breast tumor. Supplementary figure S2 shows MDA-MB-231 tumor invasion patterns in each ECM environment at day 0 and day 5. MDA-MB-231 in collagen I showed more collective invasion (supplementary figure S2(b)). But, in collagen I + fibronectin, MDA-MB-231 invasion was negligible (supplementary figure S2(c)). In collagen I + laminin, the MDA-MB-231 invasion made very thin and unusual thread-like protrusions (supplementary figure S2(d)). Based on the observation, we concluded collagen I is the good ECM condition to show breast tumor invasion and extravasation once after we added the blood endothelial channel to the system, which is fairly reasonable in that collagen I maintain a nice barrier function in BEC channels.

Next, we introduced one of the bone parenchymal cells, osteoblasts, in the 3D collagen I to mimic the bone microenvironment and breast tumor extravasation in the bones as described previously [41]. After gelation of collagen I containing 500 000 cells ml^{-1} osteoblasts, we seeded BECs into the hollow channel of the device and cultured them for 2 d on a rocker to form an engineered blood vessel in the bone microenvironment (figure 3(a)). Osteoblasts well exhibited mesenchymal cell-like, stretched morphology (figure 3(b)), evidencing that the culture condition was good enough for osteoblasts to survive and proliferate [42]. Indeed when we cultured them in a very high density (10 million ml^{-1}), we did not see any mesenchymal cell-like, stretched morphology (supplementary figure S3). Furthermore, the high dense condition induced osteoblast apoptosis, which was confirmed by immunostaining with anti-cleaved caspase 3 antibodies (supplementary figure S4). In these supplementary experiments, we did not see any issues in osteoblasts when we culture them in 500 000 cells ml^{-1} density. Furthermore, anti-Ki-67 staining on these cells in the right density confirmed that osteoblasts and other types of organ cells were thrive and proliferate well in the bulk condition (figure 4). After confirming and validating our culture condition, we introduced GFP-transfected MDA-MB-231 cells into the lumen of the engineered blood vessel to mimic circulating tumor cells that arrived at blood vessels in the bones. We maintained the experiments for 6 d and observed MDA-MB-231 cell extravasation in the bone microenvironment, which was not shown in the 'no cell' controls (figures 3(c) and (d)). The results showed that osteoblasts facilitated trans-endothelial migration of MDA-MB-231 cells from the vessel lumens to the interstitium.

3.4. Organotropic extravasation in breast cancer

Our next question was if the result in figure 3 was a generic feature of MDA-MB-231 extravasation responding to certain types of parenchymal cells in the ECM bulk or if this could be organ-specific to the bones, compared to other organs, such as the lungs. Moreover, we asked a question if this phenomenon is distinctively observed in a specific subpopulation of the MDA-MB-231 cells, including bone MDA-231 or lung MDA-231. Clearly, the bones and lungs are the most common organ sites in breast cancer metastasis [11]. To address these questions, we created

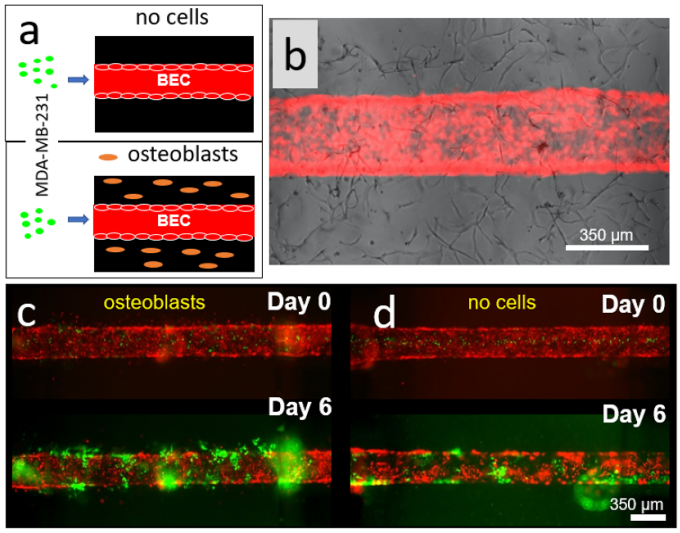

Figure 3. Osteoblast-induced breast tumor extravasation. (a) A schematic of a biomimetic blood vessel (a BEC channel, red) surrounded by ECM (black) containing no cells (top) vs. osteoblasts (orange, bottom), mimicking the control ECM vs. bone-like ECM. Next, MDA-MB-231 breast tumor cells are introduced into the vessel lumen and breast tumor extravasation is observed. (b) A representative image of morphologically elongated osteoblasts (bright-field) and a BEC channel (mApple-transfected BEC). (c)-(d) Confocal images of GFP-positive MDA-MB-231 cells introduced into engineered blood vessels (mApple-red) in the bone-like ECM (c) and control ECM (d) at day 0 (top) and day 6 (bottom) after tumor cell introduction.

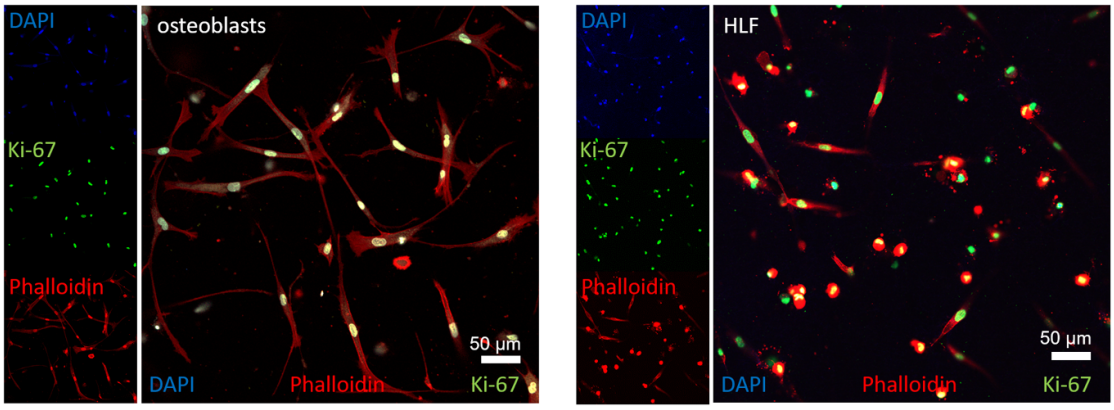

Figure 4. Assessment of organ cells in 3D collagen I. Osteoblasts (left, 0.5 million ml^{-1}) and human lung fibroblasts (HLF, right, 0.5 million ml^{-1}) in 3D collagen I were stained with anti-Ki-67 antibodies (green) to confirm organ cell survival and proliferation in the collagen I bulk. Phalloidin (in red) show stretched cell morphology.

different organ microenvironments using three different types of parenchymal cells. For mimicking the bone microenvironment, we introduced osteoblasts and bone marrow-derived MSC, respectively, in the ECM bulk. For preparing the lung microenvironment, we introduced human lung fibroblasts (HLF) in the bulk. As we mentioned before, to assess the proliferation status of the organ cells in the collagen I, the Ki-67 staining were performed (figure 4). As shown in figure 4, osteoblasts and HLF presented Ki-67 signals in green FITC florescence in their nucleus.

The vascular permeability for the blood vessels with the various ECM conditions was examined as shown in figure 5. HLF, MSC, and OST (at 500 000 cells ml^{-1}) were embedded in the collagen I. As controls, non-cell collagen I was also casted. Next, BEC were seeded into the hollow channel to form engineered vessels in different organ-like conditions. After 3 d of BEC seeding, we tested vessel permeability. When the 70 kDa dextran-FITC conjugated was perfused into the channels, no leakage was observed for 4 min in all the ECM conditions, indicating that the organ cells did not affect the vascular barrier function (figure 5).

Next we introduced tumor cells in the optimized condition (figure 6). All the parenchymal cells were introduced at the same cell seeding density (500 000 cells ml^{-1}) under the same media condition (DMEM, low glucose, 10% FBS). As a control, we included non-cell collagen I. After one day, we seeded BEC to generate an engineered blood vessel in the bone and lung microenvironments. After

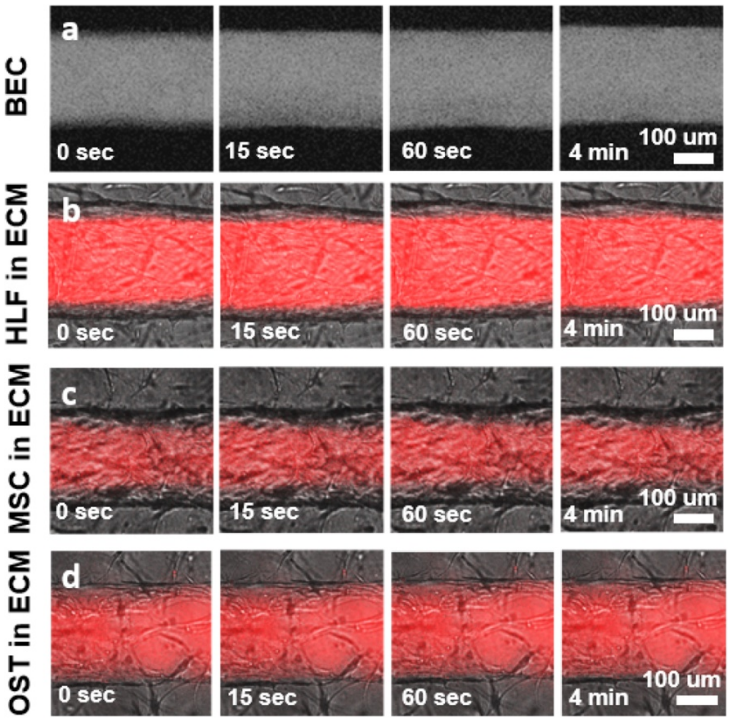

Figure 5. Vascular permeability test for various organ-like ECM environments. The 70 kDa dextran-FITC conjugated was perfused into the BEC channel in collagen I with no organ cells (a), HLF in ECM (b), MSC in ECM (c), and OST in ECM (d) to test vascular barrier function in different organ conditions. The dextran-FITC is displayed in gray in (a), in red (pseudo-colored) in the fluorescence-brightfield overlay images (b)-(d).

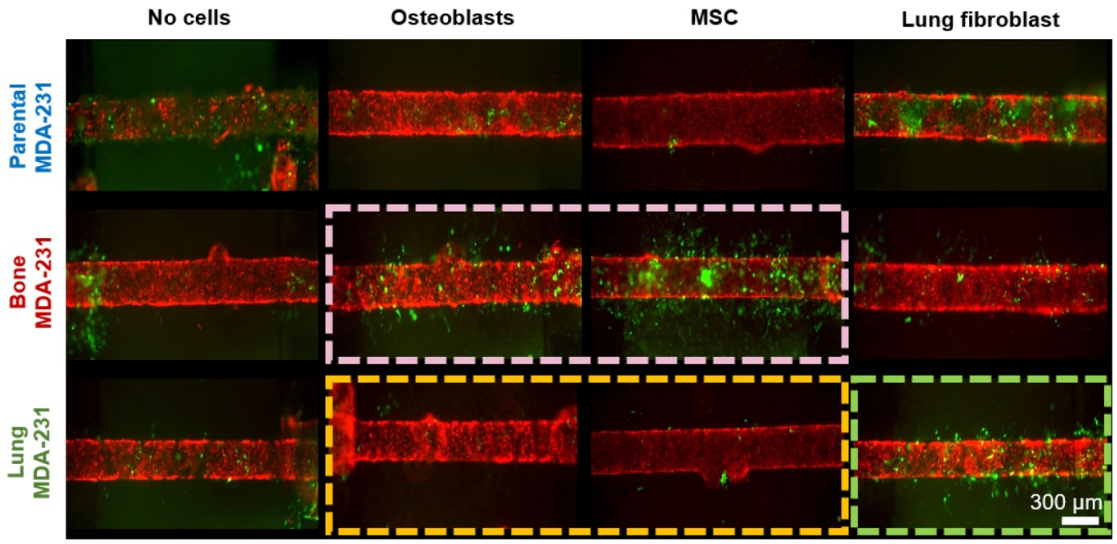

Figure 6. Organ-specific tumor metastasis 3D *in vitro*. Parental, bone-tropic, and lung-tropic MDA-MB-231 cells were introduced into blood vessels surrounded by collagen I with no cells, osteoblasts, bone-marrow derived MSC, and lung fibroblasts. The experiment was maintained for 6 d. Representative images at day 6 are presented. The highlighted boxes (pink, orange, green) indicate the organ-specific extravasations.

2 d of culture with fluid shear stress on the rocking platform for maintaining blood vascular integrity, we introduced three different MDA-MB-231 cell populations, including parental MDA-231 cells, bone MDA-231 cells, and lung MDA-231 cells, at the same density (100 000 cells ml^{-1}) into a lumen of the engineered blood vessel. The bone MDA-231 (1833 BoM [43]) and lung MDA-231 (4175 LM2 [44]) cells, donated from Dr Joan Massague, are the enriched subpopulation of MDA-MB-231 in the bones and the lungs, respectively, which was generated in MDA-MB-231 xenografts in mice.

After introducing these tumor cells to the system, we maintained the experiments for 6 d on the rocking platform. Strikingly, we found that the subpopulations of the MDA-MB-231 cells responded to the

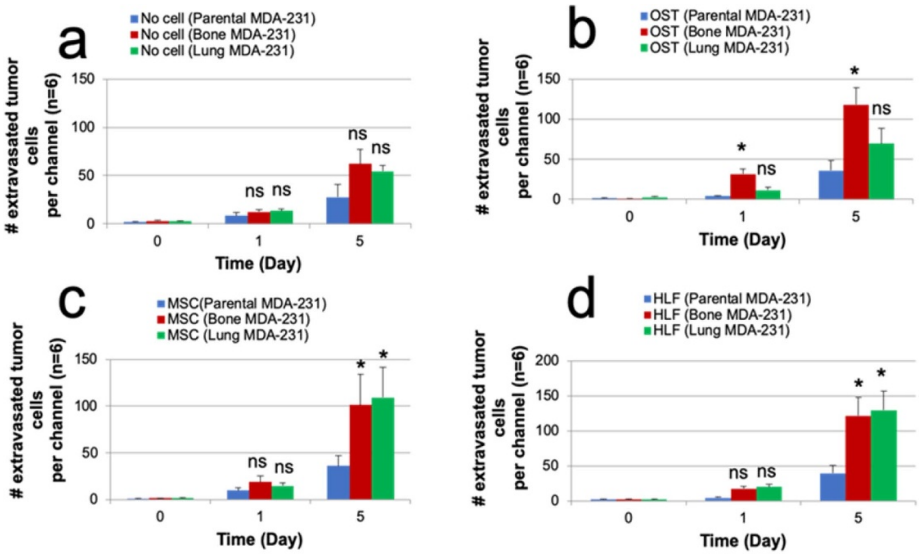

Figure 7. Comparison of organ-specific metastatic MDA-MB-231 cell extravasation. The number of each organ-specific MDA-MB-231 cells extravagated out of the blood vessels was counted in six independent channels of the same condition in ECM microenvironment with (a) no cells, (b) OST, (c) bone-marrow derived MSC, and (d) HLF. ns, statistically not significant; *, $p < 0.05$ statistically significant. Error bars depict SEM.

corresponding organ microenvironments very differently (figure 6). The bone MDA-231 cells robustly extravagated in the bone condition (osteoblasts and MSC, highlighted in a pink box in figure 6), while the lung MDA-231 did not extravagate in the bone condition (highlighted in an orange box in figure 6). However, noteworthily, the lung MDA-231 showed robust extravasation in the lung microenvironment with the HLF (highlighted in a small green box in figure 6).

Given these qualitative observations in figure 6, we repeated the experiments, and further quantified organ-specific extravasation as shown in figure 7. In each ECM microenvironment and different time points (day 0 vs. day 1 vs. day 5), the numbers of organ-specific MDA-231 cells extravagated out of the engineered blood vessels were counted in six independent experiments ($n = 6$). At day 1, non-cell ECM showed minimal extravasation with any types of MDA-MB-231 cells (parental, bone, and lung MDA-231) (figure 7(a), day 1). In the OST condition, bone MDA-231 cells showed higher extravasation, compared to parental MDA-231 and lung MDA-231 cells (figure 7(b), day 1). In the MSC condition, we observed similar trends of extravasation to those in the OST group, but MSC data was not statistically significant at day 1 (figure 7(c), day 1). In the lung microenvironment with HLF, we did not see any difference between the bone MDA-231 and lung MDA-231 at day 1 (figure 7(d), day 1).

At day 5, non-cell ECM controls did not show any significant differences in extravasation in any type of MDA-231 cells, though metastatic bone or lung MDA-231 cells showed commonly increased extravasation compared to parental MDA-231 cells (figure 7(a), day 5). In the OST condition, bone MDA-231 cells showed superior extravasation, compared to parental MDA-231 and lung MDA-231 cells at day 5 (figure 7(b), day 5). Interestingly, in either MSC or HLF condition (figures 7(c) and (d); day 5), both the bone MDA-231 and lung MDA-231 cells extravagated robustly. These data suggest that MSC and HLF could promote either/both proliferation or/and migration generally in those subpopulations of the MDA-MB-231 tumor cells.

In summary, our studies show that our new method and 3D co-culture system can provide a unique platform to isolate organ-specific metastases *in vitro*, which need to be further investigated *in vivo*. Also, the study reveals that osteoblasts play a role in selective extravasation of the bone metastatic tumor cells among other subtypes of MDA-MB-231, such as lung MDA-231 cells. Furthermore, these organ cells did not disrupt vascular barrier, which implies that osteoblasts may have unknown, but important roles in breast tumor bone metastasis and/or organotropic selection of the bone metastases in TNBC. Further investigations on the secretome of these organ cells and their crosstalk with tumor cells would lead to the potential translational use of the factors or signals to defeat breast cancer metastasis.

4. Conclusions

In this study, we presented a rapid multilayer microfabrication methodology to reproducibly generate a 3D engineered blood vasculature surrounded by organ-specific parenchymal cells, which enabled us to study breast tumor extravasation in different organ

microenvironments. The process was carried out by producing a vascular channel with a single casting mold by transferring a 3D overhang pattern made through the novel two-layer SU-8 photolithography process to a substrate with a sacrificial layer. This technology allowed to investigate breast tumor extravasation in distinct organs, including bones and lungs, the major pre-metastatic organs in breast cancer, to recapitulate the critical step in the organotropic metastasis. Our study showed that osteoblasts play a pivotal role in selective extravasation of the bone MDA-231 among other breast tumor subpopulations. Moreover, the findings suggest that further investigations into the roles of the osteoblast-mediated factors and signals in promoting bone metastasis are warranted. In this study, we emphasize the utility of our new biomaterial platform and fabrication method to investigate crosstalk among human vasculatures, organ cells, and tumor cells rapidly and reproducibly.

Acknowledgments

T.J.K. and E.L. are supported by the Cornell University Start-up funds, and the Nancy and Peter Meinig Family Investigator funds. This work was performed in part at the Cornell NanoScale Facility (CNF), a member of the National Nanotechnology Coordinated Infrastructure (NNCI), which is supported by the National Science Foundation (Grant No. NNCI-1542081). The authors thank to Dr Joan Massague for kindly donating his bone tropic and lung tropic breast cancer cell lines. The authors also thank Dr Tao Luo and Thomas Pennell for valuable discussions on the topic.

Conflicts of interest

There are no conflicts to declare.

ORCID iDs

Tae Joon Kwak https://orcid.org/0000-0003-1669-1996
Esak Lee https://orcid.org/0000-0002-5328-6677

References

[1] DeSantis C E, Ma J, Gaudet M M, Newman L A, Miller K D, Goding Sauer A, Jemal A and Siegel R L 2019 Breast cancer statistics, 2019 *CA Cancer J. Clin.* **69** 438–51
[2] Foulkes W D, Smith I E and Reis-Filho J S 2010 Triple-negative breast cancer *New Engl. J. Med.* **363** 1938–48
[3] Lee E, Fertig E J, Jin K, Sukumar S, Pandey N B and Popel A S 2014 Breast cancer cells condition lymphatic endothelial cells within pre-metastatic niches to promote metastasis *Nat. Commun.* **5** 4715
[4] Henderson A R, Choi H and Lee E 2020 Blood and lymphatic vasculatures on-chip platforms and their applications for organ-specific *in vitro* modeling *Micromachines* **11** 147
[5] Folkman J 1971 Tumor angiogenesis: therapeutic implications *New Engl. J. Med.* **285** 1182–6
[6] Senger D R, Galli S J, Dvorak A M, Perruzzi C A, Harvey V S and Dvorak H F 1983 Tumor cells secrete a vascular permeability factor that promotes accumulation of ascites fluid *Science* **219** 983–5
[7] Lee E, Koskimaki J E, Pandey N B and Popel A S 2013 Inhibition of lymphangiogenesis and angiogenesis in breast tumor xenografts and lymph nodes by a peptide derived from transmembrane protein 45A *Neoplasia* **15** 112–24
[8] Lee E, Lee S J, Koskimaki J E, Han Z, Pandey N B and and Popel A S 2014 Inhibition of breast cancer growth and metastasis by a biomimetic peptide *Sci. Rep.* **4** 7139
[9] Lee E, Song H G and Chen C S 2016 Biomimetic on-a-chip platforms for studying cancer metastasis *Curr. Opin. Chem. Eng.* **11** 20–27
[10] Lee E, Pandey N B and Popel A S 2015 Crosstalk between cancer cells and blood endothelial and lymphatic endothelial cells in tumour and organ microenvironment *Expert Rev. Mol. Med.* **17** e3
[11] Patanaphan V, Salazar O M and Risco R 1988 Breast cancer: metastatic patterns and their prognosis *South Med. J.* **81** 1109–12
[12] Lu X and Kang Y 2007 Organotropism of breast cancer metastasis *J. Mammary Gland Biol. Neoplasia* **12** 153–62
[13] Lambert A W, Pattabiraman D R and Weinberg R A 2017 Emerging biological principles of metastasis *Cell* **168** 670–91
[14] Lawson D A, Kessenbrock K, Davis R T, Pervolarakis N and Werb Z 2018 Tumour heterogeneity and metastasis at single-cell resolution *Nat. Cell Biol.* **20** 1349–60
[15] Stuelten C H, Parent C A and Montell D J 2018 Cell motility in cancer invasion and metastasis: insights from simple model organisms *Nat. Rev. Cancer* **18** 296–312
[16] Lee E, Pandey N B and Popel A S 2014 Pre-treatment of mice with tumor-conditioned media accelerates metastasis to lymph nodes and lungs: a new spontaneous breast cancer metastasis model *Clin. Exp. Metastasis* **31** 67–79
[17] Perel P, Roberts I, Sena E, Wheble P, Briscoe C, Sandercock P, Macleod M, Mignini L E, Jayaram P and Khan K S 2007 Comparison of treatment effects between animal experiments and clinical trials: systematic review *BMJ* **334** 197
[18] Baker B M and Chen C S 2012 Deconstructing the third dimension: how 3D culture microenvironments alter cellular cues *J. Cell Sci.* **125** 3015–24
[19] Benam K H *et al* 2015 Engineered *in vitro* disease models *Ann. Rev. Pathol.: Mech. Dis.* **10** 195–262
[20] Nguyen D-H T, Stapleton S C, Yang M T, Cha S S, Choi C K, Galie P A and Chen C S 2013 Biomimetic model to reconstitute angiogenic sprouting morphogenesis *in vitro* *Proc. Natl Acad. Sci.* **110** 6712–7
[21] Nguyen D-H T, Lee E, Alimperti S, Norgard R J, Wong A, Lee J J K, Eyckmans J, Stanger B Z and Chen C S 2019 A biomimetic pancreatic cancer on-chip reveals endothelial ablation via ALK7 signaling *Sci. Adv.* **5** eaav6789
[22] Polacheck W J, Kutys M L, Tefft J B and Chen C S 2019 Microfabricated blood vessels for modeling the vascular transport barrier *Nat. Protocols* **14** 1425–54
[23] Li X, Xia J, Nicolescu C T, Massidda M W, Ryan T J and Tien J 2018 Engineering of microscale vascularized fat that responds to perfusion with lipoactive hormones *Biofabrication* **11** 014101
[24] Kwak T J and Lee E 2020 *In vitro* modeling of tumor spheroid interactions to perfused blood vessels (accepted)
[25] Kolesky D B, Homan K A, Skylar-Scott M A and Lewis J A 2016 Three-dimensional bioprinting of thick vascularized tissues *Proc. Natl Acad. Sci.* **113** 3179–84
[26] Mirabella T, MacArthur J W, Cheng D, Ozaki C K, Woo Y J, Yang M T and Chen C S 2017 3D-printed vascular networks direct therapeutic angiogenesis in ischaemia *Nat. Biomed. Eng.* **1** 0083

[27] Han X, Bibb R and Harris R 2016 Engineering design of artificial vascular junctions for 3D printing *Biofabrication* **8** 025018
[28] Li X, Liu L, Zhang X and Xu T 2018 Research and development of 3D printed vasculature constructs *Biofabrication* **10** 032002
[29] Yang L, Shridhar S V, Gerwitz M and Soman P 2016 An *in vitro* vascular chip using 3D printing-enabled hydrogel casting *Biofabrication* **8** 035015
[30] Bischel L L, Young E W K, Mader B R and Beebe D J 2013 Tubeless microfluidic angiogenesis assay with three-dimensional endothelial-lined microvessels *Biomaterials* **34** 1471–7
[31] Herland A, van der Meer A D, FitzGerald E A, Park T-E, Sleeboom J J F and Ingber D E 2016 Distinct contributions of astrocytes and pericytes to neuroinflammation identified in a 3D human blood-brain barrier on a chip *PloS One* **11** e0150360
[32] Sano H, Watanabe M, Yamashita T, Tanishita K and Sudo R 2020 Control of vessel diameters mediated by flow-induced outward vascular remodeling *in vitro Biofabrication* **12** 045008
[33] Kang Y, Siegel P M, Shu W, Drobnjak M, Kakonen S M, Cordón-Cardo C, Guise T A and Massagué J 2003 A multigenic program mediating breast cancer metastasis to bone *Cancer Cell* **3** 537–49
[34] Minn A J, Gupta G P, Siegel P M, Bos P D, Shu W, Giri D D, Viale A, Olshen A B, Gerald W L and Massagué J 2005 Genes that mediate breast cancer metastasis to lung *Nature* **436** 518–24
[35] Bohl B, Steger R, Zengerle R and Koltay P 2005 Multi-layer SU-8 lift-off technology for microfluidic devices *J. Micromech. Microeng.* **15** 1125–30
[36] Pinto V C, Sousa P J, Cardoso V F and Minas G 2014 Optimized SU-8 processing for low-cost microstructures fabrication without cleanroom facilities *Micromachines* **5** 738–55
[37] Kwak T J, Nam Y G, Najera M A, Lee S W, Strickler J R and Chang W-J 2016 Convex grooves in staggered herringbone mixer improve mixing efficiency of laminar flow in microchannel *PloS One* **11** e0166068
[38] Lee J N, Park C and Whitesides G M 2003 Solvent compatibility of poly(dimethylsiloxane)-based microfluidic devices *Anal. Chem.* **75** 6544–54
[39] Lee J-H, Choi W-S, Lee K-H and Yoon J-B 2008 A simple and effective fabrication method for various 3D microstructures: backside 3D diffuser lithography *J. Micromech. Microeng.* **18** 125015
[40] Fenech M, Girod V, Claveria V, Meance S, Abkarian M and Charlot B 2019 Microfluidic blood vasculature replicas using backside lithography *Lab Chip* **19** 2096–106
[41] Bersini S, Jeon J S, Dubini G, Arrigoni C, Chung S, Charest J L, Moretti M and Kamm R D 2014 A microfluidic 3D *in vitro* model for specificity of breast cancer metastasis to bone *Biomaterials* **35** 2454–61
[42] Skottke J, Gelinsky M and Bernhardt A 2019 *in vitro* co-culture model of primary human osteoblasts and osteocytes in collagen gels *Int. J. Mol. Sci.* **20** 1998
[43] Zhang X H, Wang Q, Gerald W, Hudis C A, Norton L, Smid M, Foekens J A and Massague J 2009 Latent bone metastasis in breast cancer tied to Src-dependent survival signals *Cancer Cell* **16** 67–78
[44] Minn A J *et al* 2007 Lung metastasis genes couple breast tumor size and metastatic spread *Proc. Natl Acad. Sci. USA* **104** 6740–5